

Probing S4 and S5 segment proximity in mammalian hyperpolarization-activated HCN channels by disulfide bridging and Cd^{2+} coordination

Damian C. Bell · Harma K. Turbendian ·
Matthew T. Valley · Lei Zhou · John H. Riley ·
Steven A. Siegelbaum · Gareth R. Tibbs

Received: 6 August 2008 / Accepted: 30 October 2008 / Published online: 26 November 2008
© The Author(s) 2008. This article is published with open access at Springerlink.com

Abstract We explored the structural basis of voltage sensing in the HCN1 hyperpolarization-activated cyclic nucleotide-gated cation channel by examining the relative orientation of the voltage sensor and pore domains. The

opening of channels engineered to contain single cysteine residues at the extracellular ends of the voltage-sensing S4 (V246C) and pore-forming S5 (C303) domains is inhibited by formation of disulfide or cysteine: Cd^{2+} bonds. As Cd^{2+} coordination is promoted by depolarization, the S4–S5 interaction occurs preferentially in the closed state. The failure of oxidation to catalyze dimer formation, as assayed by Western blotting, indicates the V246C:C303 interaction occurs within a subunit. Intriguingly, a similar interaction has been observed in depolarization-activated *Shaker* voltage-dependent potassium (Kv) channels at depolarized potentials but such an intrasubunit interaction is inconsistent with the X-ray crystal structure of Kv1.2, wherein S4 approaches S5 of an adjacent subunit. These findings suggest channels of opposite voltage-sensing polarity adopt a conserved S4–S5 orientation in the depolarized state that is distinct from that trapped upon crystallization.

Electronic supplementary material The online version of this article (doi:10.1007/s00424-008-0613-3) contains supplementary material, which is available to authorized users.

D. C. Bell · M. T. Valley · L. Zhou · J. H. Riley · S. A. Siegelbaum
Departments of Neuroscience,
College of Surgeons and Physicians, Columbia University,
722 West 168th Street,
New York, NY 10032, USA

S. A. Siegelbaum
e-mail: sas8@columbia.edu

H. K. Turbendian · G. R. Tibbs (✉)
Departments of Anesthesiology,
College of Surgeons and Physicians, Columbia University,
New York, NY 10032, USA
e-mail: grt1@columbia.edu

S. A. Siegelbaum · G. R. Tibbs
Departments of Pharmacology,
College of Surgeons and Physicians, Columbia University,
New York, NY 10032, USA

S. A. Siegelbaum
The Howard Hughes Medical Institute,
College of Surgeons and Physicians, Columbia University,
New York, NY 10032, USA

Present address:

D. C. Bell
Ion Channel Group, AstraZeneca,
Alderley Park,
Macclesfield SK10 4TG, UK

Keywords HCN clones · Pacemaker · Voltage gating · Cysteine · Cross-bridge

Introduction

The hyperpolarization-activated cyclic nucleotide-gated (HCN) cation channels are unusual among voltage-gated cation channels in that they activate upon membrane hyperpolarization. This enables them to open following repolarization of the action potential, where they generate an inward Na^+ current that contributes to the spontaneous pacemaker depolarization in cardiac myocytes and certain neurons [41, 46]. Despite their atypical polarity of gating, HCN channels are homologous to the six-transmembrane-segment (S1–S6) depolarization-activated voltage-dependent

potassium (Kv) channels. Thus, in both HCN [34, 45] and Kv channels [1, 6, 28, 30, 32, 37], the S4 transmembrane helix shows a highly conserved pattern of positively charged amino acids at every third residue; this positive charge is critical in sensing transmembrane voltage changes that lead to channel activation. Similarly, there are notable sequence similarities between HCN and Kv channels in the S5, S6, and reentrant P loop motif that form the ion-conducting pore [3, 19, 34, 45]. The basis of the opposite polarity of voltage gating in the face of this overall conservation of architecture is, thus, intriguing.

The motions of the positively charged S4 transmembrane helices during voltage sensing that lead to channel gating are still controversial, despite over two decades of research on voltage-sensitive channels (inclusive of ion channels across the superfamilies of Kv, Nav, and Cav; for reviews, see [17, 49]). From this wealth of data, three quite different putative models of voltage sensing are emerging, broadly grouped according to the translational motion of S4 through and relative to the transmembrane electric field. The “transporter model” involves limited translational motions ($\sim 2\text{--}4\text{ \AA}$), often accompanied by a twist of the S4 helix, through a narrow focused electric field created by deformations of, and aqueous crevices into, the lipid membrane around the S4 helix [2, 6, 7, 13, 14, 20, 39, 48, 51, 52]. In a second model type, the “helical screw model”, the S4 helix translates $\sim 5\text{--}14\text{ \AA}$ (depending on the modeled angle of tilt of S4) perpendicular to the plane of the lipid bilayer, a motion often accompanied by a 180° rotation of the helix [4, 9, 12, 22, 26, 38, 53]. Finally, the “paddle model”, largely derived from a series of crystal structures and functional current analyses from the MacKinnon lab, depicts S4, in concert with transmembrane helix S3b (together forming the paddle structure), moving from a prone/tilted position to an upright/vertical position in the membrane electric field, with a translational motion of $\sim 15\text{--}20\text{ \AA}$ [23, 33, 43].

Even among the limited members of the hyperpolarization-activated HCN channel family, no single consensus model fits the different S4 motions observed, and data exemplifying characteristics of each of the three models of S4 voltage sensing movements have been described. Thus, in the sea urchin spHCN channel S4 motions resemble the helical screw model [35]; while motions in the plant hyperpolarization-activated KAT1 channel [21, 24] suggest a paddle model (although S4 translational distances are shorter at $\sim 12\text{--}15\text{ \AA}$). In both the bacterial methanococcal voltage-gated potassium channel [47] and mammalian HCN channels [5, 50], the data are most readily explained by the transporter model wherein S4 undergoes a limited translational motion in the confines of aqueous crevices.

One approach that can shed light on dynamic rearrangements in channels is through the assay of disulfide bond

formation or metal ion coordination between pairs of cysteine residues localized in different regions of the channel. Depending on the thermal energy present, Cys–Cys disulfide bridges only arise if the Cys residues are within 15 \AA of each other [10], while Cd^{2+} coordination between two or more Cys residues further restricts the molecular proximity to $<6\text{ \AA}$ [11, 42]. With this approach, it has been shown that the extracellular end of the Kv S4 lies within 6 \AA of the extracellular end of S5 of a neighboring subunit, suggesting a close intersubunit proximity [8, 25, 36]. However, there is also evidence that similar residue positions on Kv S4 and S5 within the same subunit interact to coordinate Cd^{2+} , suggesting a close intrasubunit proximity. For example, Elliott et al. [18] reported a state-dependent change in the orientation of S4 relative to S5. Using tandem dimers of concatenated *Shaker* Kv channel subunits to fix the stoichiometry of inserted Cys residues on S4 and S5, they showed that both intra- and intersubunit S4 to S5 disulfide bonds could form upon exposure to the catalytic agent copper (II)-phenanthroline (CuPhen). Further, by inference from these tandem dimer experiments, they concluded that in the resting state of the Kv channel, when the membrane is hyperpolarized, the top of S4 lies near the top of S5 in an adjacent subunit, enabling the formation of an *intersubunit* Cd^{2+} coordination site. In contrast, following channel activation in response to depolarization, the orientation of S4 changes so that its extracellular end now lies near the extracellular end of the S5 segment in the same subunit, permitting the formation of an *intrasubunit* Cd^{2+} coordination site. Furthermore, using the hyperpolarization-activated KAT1 channel, the Jan laboratory performed elegant helix packing studies and provided evidence for close atomic proximities for three sets of residue pairings between S4 and S5 [21, 24]. They suggest that two of these pairings are intrasubunit whereas the third is intersubunit. However, these S4 to S5 intra- and intersubunit interactions are inferred from a model based on the Kv1.2 crystal structure [31] and, thus, do not provide direct evidence to discriminate between intra- and intersubunit interactions.

Here, we explore the proximity of the extracellular ends of S4 and S5 in a minimal HCN1 channel (HCN1-R) engineered to remove all but one endogenous cysteine residue (C303) that is located near the extracellular end of S5 and is essential for channel function [5]. We find that when a cysteine was substituted for valine 246 at the external, N-terminal side of the HCN1-R S4 segment, the resulting channels demonstrate robust formation of disulfide bonds or Cys:metal ion bridges. Generation of either of these linkages stabilizes the closed state of the channel, shifting voltage gating to more hyperpolarized potentials. Consistent with this, the rate of modification of gating by Cd^{2+} is enhanced when the membrane is depolarized so that

the channels are in the deactivated closed state. Biochemical experiments support the hypothesis that these functional effects are mediated via formation of intrasubunit interactions between V246C and C303. These results suggest HCN and Kv channels (cf. 18) can adopt similar conformations at depolarized potentials, in which the externally facing ends of S4 and S5 on the same subunit lie in close proximity. This implies that the relative orientation of the voltage sensor and pore domains in the deactivated conformation of HCN channels resembles the orientation of these domains in the activated conformation of Kv channels.

Materials and methods

Molecular biology

Our experiments were performed in the background of a near cysteine-free channel, HCN1-R, which has a single endogenous Cys residue at position 303, as previously described [5]. In brief, HCN1-R has a truncation at the end of S6, resulting in the deletion of the entire cytoplasmic C-terminus and removal of six out of twelve endogenous Cys residues in full-length HCN1. Five of the six remaining Cys were replaced using the following substitution mutations: C55S, C298I, C318S, C347S, and C374T. Mutation of C303 in the S5 segment to any one of the other 19 amino acids failed to yield functional channels. HCN1-R displayed normal hyperpolarization-activated gating and was *resistant* to modification by a variety of sulfhydryl-reactive reagents (for more information, see [5]). An individual Cys substitution, V246C, was made at the external NH₂-terminal end of the S4 region of HCN1-R using polymerase chain reaction mutagenesis. All constructs were subcloned into the pGEM-HE vector [29] and verified using dideoxy chain termination sequencing. RNA was transcribed from *NheI*-linearized DNA using a T7 RNA polymerase (Message Machine, Applied Biosystems). RNA concentration was measured from the optical density ratio at 260 and 280 nm wavelengths [44] using a DU640 spectrophotometer (Beckman, CA, USA).

Animal procedures and cell culture

Xenopus laevis oocytes were harvested according to a Columbia University approved protocol (PI#366G CU#2928). Of cRNA (0.5 µg/µl), 50 nl were injected into each oocyte and cells were maintained in Barth's solution (Specialty Media) in the absence or presence of 0.15 mM dithiothreitol (DTT) as indicated. Media was changed every 24 h.

Electrophysiology

Two-electrode voltage clamp (TEVC) recordings were routinely performed 48 h after oocyte injection. Data was acquired using an OC-725C voltage-clamp amplifier (Warner Instrument Corp.), filtered at 1 kHz using an eight-pole low pass Bessel filter (Frequency Devices) and sampled at 2 kHz using an ITC16 interface (InstruTech Corp.) controlled by Pulse software (HEKA Elektronik). No linear leak subtraction was applied to current recordings. In representative sweeps, the capacity transients are truncated for clarity. The extracellular solution contained (in mM) 112 KCl, 2 MgCl₂, 10 4-(2-hydroxyethyl)-1-piperazineethanesulfonic acid, and pH 7.4 (KOH). Microelectrodes were filled with 3 M KCl and had resistances of 0.5–3 MΩ. Ag–AgCl grounding wires were isolated from bath solutions by 3 M KCl/2% agar bridge electrodes. All recordings were performed at room temperature (21–24°C).

Voltage clamp paradigms and analysis

In all voltage clamp experiments, the holding potential was –20 mV. To measure steady-state gating parameters, tail current amplitudes were determined upon repolarization to the holding potential after stepping for 3 s to hyperpolarizing test potentials applied in –10 mV intervals from –25 mV. The relationship between peak tail current and test potential was plotted and the resulting current–voltage (*I*–*V*) relationship was fitted with the Boltzmann equation (Eq. 1):

$$I(V) = A_1 + A_2 / \{1 + \exp[(V - V_{1/2})/s]\} \quad (1)$$

where A_1 is an offset due to the holding current, A_2 is the maximal tail current amplitude, $V_{1/2}$ is the midpoint activation voltage, and s is the slope factor of the relation (mV). Mean tail current activation curves were obtained by subtracting the offset (A_1) from individual current–voltage curves and then normalizing by the maximal amplitude (A_2). The normalized data were then averaged among different experiments and the mean normalized tail *I*–*V* relation fitted with the Boltzmann equation.

To determine the state dependence of the kinetics of inhibition by Cd²⁺, current amplitudes were monitored in response to 3-s steps to –125 mV applied at different frequencies during the application of Cd²⁺. A protocol in which a strong 3-s hyperpolarization was applied once every 4 s was used to determine the rate of Cd²⁺ block when channels were largely in the open state cycle (channels open for ~75% of the duty cycle). A protocol in which a 3-s hyperpolarization was applied once every 24 s was used to measure the rate of Cd²⁺ block when channels were biased toward the closed state (channels closed for

87.5% of the duty cycle). Peak currents were measured before, during, and after application of Cd^{2+} (at the indicated concentrations) in the bath solution and plotted against the duration of the Cd^{2+} application. The measured currents were normalized to the control current prior to Cd^{2+} perfusion. The Cd^{2+} inhibition (coordination) time constant was determined by fitting a single exponential to the current decay on application of Cd^{2+} . The Cd^{2+} unblock (recovery) time constant was determined by fitting a single exponential to the growth of current (Cd^{2+} unblock) on wash-off of applied Cd^{2+} .

Analyses were performed using PulseFit (v8.5, HEKA Elektronik) and Microcal Origin software (v6.0, Microcal Software, Inc.). Statistical analysis was performed using paired or unpaired Student's *t* tests and one-way analysis of variance (ANOVA) as indicated. Differences were considered significant if *p* was less than 0.05.

Preparation of *Xenopus* oocyte lysates for biochemical analysis

Forty-eight hours after cRNA injection, batches of 20–50 oocytes were washed with 2×5 ml of DTT-free ice-cold Barth's solution, incubated at room temperature for 3 min in Barth's solution containing either no addition or CuPhen (30 μM , prepared as described below), followed by 2×5 ml washes in ice-cold Barth's solution. Cells were then immediately disrupted under a nitrogen atmosphere by sonication (CP130 Ultrasonic processor, Cole Parmer) in 20 μl per cell of ice cold, nitrogen purged (bubbled with N_2 for 2 h on ice before use) 3-[(3-cholamidopropyl)dimethylammonio]-1-propanesulfonate (CHAPS) lysis buffer that was prepared fresh on day of use and contained 1% CHAPS, 20 mM *N*-ethylmaleimide (NEM), 2 mM ethylene glycol tetraacetic acid, 2 mM ethylenediaminetetraacetic acid (EDTA), 100 mM NaF, 10 mM Na_2MoO_4 , 50 mM Tris base, 2 mM Na_3VO_4 , 10 mM $\text{Na}_4\text{P}_2\text{O}_7$, 1 mM phenylmethylsulfonyl fluoride (PMSF), and pH adjusted to 7.0 with HCl and with one "CompleteMini" protease inhibitor tablet per 7.5 ml final volume. Following sonication, the lysate was mixed at 4°C for 90 min on a rotary shaker. Solubilized protein was recovered by centrifugation (4×5 min at 13,000 rpm in an Eppendorf microfuge). Lysates were stored at -80°C until analyzed by polyacrylamide gel electrophoresis (PAGE) and Western blotting.

PAGE and Western blotting

Aliquots of lysates corresponding to 0.3 oocytes were denatured in PAGE loading buffer (62.5 mM Tris-HCl pH 6.8, 1 mM EDTA- Na_2 , 5% sucrose, 0.0125% bromophenol blue, 2.5% sodium dodecyl sulfate (SDS)) at 95–100°C for 2 min then separated on 12% polyacrylamide

gels using standard Laemmli electrophoresis buffers. To determine whether any higher molecular weight (MW) bands on the gels represent multimeric proteins formed by cross-linking of monomers through disulfide bonds, we ran reducing gels in which the loading buffer was supplemented with 10 mM DTT. After separation, proteins were transferred to polyvinylidene fluoride membranes using an alkaline (10 mM 3-[cyclohexylamino]-1-propane-sulfonic acid pH 11 plus 0.01% SDS), low current (90 mA, 20 h), and transfer protocol. All electrophoresis steps were performed using a miniprotean 3 system (Biorad).

Following transfer, the membranes were washed three times in $1 \times$ Tris-buffered saline (TBS) followed by 15 s in methanol. After air drying for 15 min, the positions of the dual color molecular weight markers were recorded using a rabbit antigen pen (Alpha Diagnostics). Membranes were rewetted by immersion in methanol (15 s) followed by three washes in $1 \times$ TBS. Membranes were then blocked overnight at 4°C followed by a further 90 min at room temperature. All subsequent incubations and washes were at room temperature. Blocking and binding was performed in $1 \times$ TBS-T 2% bovine serum albumin (BSA; $1 \times$ TBS supplemented with 0.05% Tween-20 and 2% BSA). Washes were performed with either $1 \times$ TBS or $1 \times$ TBS-T 0.2% BSA ($1 \times$ TBS supplemented with 0.05% Tween-20 and 0.2% BSA) as indicated below.

Membranes were incubated with the rabbit anti-HCN1 primary antibody (APC-056 obtained from Alomone Labs and applied at 100 ng/ml for 60 min) and with the horseradish peroxidase-conjugated goat antirabbit secondary antibody (20,320 from Alpha Diagnostics applied at 2 ng/ml) with six washes in $1 \times$ TBS-T 0.2% BSA following each antibody application. The blot was developed using SuperSignal West Femto (Pierce Biotechnology) and imaged using Labworks version 4.0.0.8 and an Epichem³ Darkroom (UVP BioImaging Systems). Sequential images were collected between 0.1 and 3,000 s at approximately half log intervals of time using a 2×2 binning and $0 \times$ gain. The longest exposure that did not result in saturation was chosen for densitometric analysis using LabWorks. The density of bands in sample lanes were corrected for background by subtracting the density of size and position matched areas in lanes where uninjected lysate samples were run. Images for display were exported from LabWorks at a bin range of 0–255 with no other image processing then imported into Adobe Illustrator version 10.0.3 (Adobe Systems) where they were scaled and the contrast inverted but the image not otherwise altered.

Molecular modeling

A sequence alignment between the Kv1.2–Kv2.1 chimera [33] and mHCN1 (see online supplemental data) based on a

combination of a primary protein sequence alignment program (Clustal W), transmembrane topology predictions (TMHMM, TM-pred, SOSUI, <http://ca.expasy.org/tools/>), and visual inspection. Modeler (8v1, <http://salilab.org/modeller/>) was used to generate the homology model of the HCN1 channel, based on the sequence alignment, and the crystal structure of Kv1.2–Kv2.1 chimera (2R9R) [33].

Reagents

Unless otherwise indicated, all reagents were from Sigma Aldrich and were of the highest available purity. Cadmium chloride was stored at 4°C as a 1-M stock made with double distilled water. Copper (II)-phenanthroline was prepared fresh on day of use from stock solutions of CuSO₄ and phenanthroline that were each stored at –20°C. After combining the reagents to final concentrations of 30 μM CuSO₄ and 90 μM phenanthroline, the solution was incubated at room temperature for at least 10 min then used within 4 h. DTT, NEM, Na₄P₂O₇, and “CompleteMini” protease inhibitors (Roche Diagnostics) were dissolved on the day of use into water, ethanol, water, and lysis buffer, respectively. All other reagents were prepared as stock solutions and kept at 4°C except for PMSF and Na₃VO₄ which were kept at –20°C. SDS (BP1311-1 nuclease and protease free) and methanol (BP1105-4 Biotech Grade) were from Fisher Scientific. Dual color molecular weight markers were from Biorad. Fraction V protease-free BSA (03-117-332-001) was from Roche.

Results

Spontaneous disulfide bond formation in V246C channels

We focused our studies on the HCN1-R channel, in which all 12 endogenous cysteine residues in HCN1 were eliminated except for Cys303 which is located in the S5 transmembrane helix and is necessary for channel function (see “Materials and methods” and [5]). Exposure of oocytes expressing HCN1-R to the reducing agent DTT for 3 min produced no functional changes in HCN1-R currents. Thus, the midpoint voltage of activation (mean $V_{1/2}$ = –77.6 mV, n = 4; see Fig. 1a) and slope factor (mean s = 7.9 mV) of the tail current activation curve before exposure to DTT are not different (p > 0.05—see legend to Fig. 1) from the respective values after exposure to the reducing agent ($V_{1/2}$ = –79.3, s = 8.3 mV, n = 4; see Fig. 1a). The failure of DTT to alter channel properties suggests that C303 may fail to form intersubunit disulfide bonds spontaneously.

V246C channels (containing two Cys residues, V246C and C303, per subunit) displayed a more negative $V_{1/2}$ (mean $V_{1/2}$ = –90.6 mV, n = 10) and reduced steepness of

activation (mean s = 13.4 mV) compared to HCN1-R under control conditions. Importantly, and in contrast to HCN1-R, application of DTT significantly enhanced V246C channel opening, shifting the $V_{1/2}$ to more positive potentials by approximately +10 mV and increasing the steepness of the activation curve ($V_{1/2}$ = –80.7 mV and s = 10.1, n = 10; p < 0.001 for both parameters; Fig. 1b). These results suggest that V246C channels spontaneously form a disulfide bond that inhibits channel opening and that the reduction of this bond by DTT reverses this inhibitory effect. Indeed, the voltage dependent gating of V246C channels in the presence of DTT is very similar to that of HCN1-R channels, indicating that the main effect of the V246C mutation is to promote disulfide bond formation, rather than to alter the energetics of channel gating by itself.

Cu-phenanthroline promotes disulfide bridging in V246C channels

To investigate further the ability of V246C channels to form a disulfide bond, we applied CuPhen, a weak oxidizing reagent known to promote Cys–Cys disulfide bridges in proteins where unbridged Cys residues lie in sufficiently close proximity. We first pretreated HCN1-R and V246C channels with DTT (0.15 mM in culture medium—see “Materials and methods”) to reverse any spontaneous disulfide bridges and then applied CuPhen (30 μM, for 2 min). HCN1-R channels showed no response to the reagent, with the mean $V_{1/2}$ and slope under control conditions (–73.2 and 8.8 mV, n = 4) similar to values determined after exposure to CuPhen (–73.3 and 8.5 mV, n = 4; p > 0.05; Fig. 2a), suggesting that C303–C303 intersubunit disulfide bonds could not form, even upon addition of the catalytic agent. In V246C channels, however, CuPhen produced a robust inhibitory effect on channel opening, shifting the $V_{1/2}$ by approximately 20 mV to more hyperpolarized potentials, the opposite of the effect seen with DTT (mean $V_{1/2}$ before and after exposure to CuPhen were –75.1 and –95.9 mV, n = 5; p < 0.01; Fig. 2b). Evidence that this effect of CuPhen is due to disulfide bond formation comes from the finding that subsequent perfusion of DTT was able to reverse the effects of CuPhen on channel activation, with the $V_{1/2}$ shifting back to close to its original control value (mean $V_{1/2}$ = –82 mV, n = 5; Fig. 2b).

The above observations suggest that one or more pairs of Cys residues in V246C channels must lie in close proximity when the channels are closed. Furthermore, the fact that CuPhen treatment of previously reduced channels produces a larger voltage shift (–20 mV) than that seen upon acute DTT treatment of channels maintained in the absence of DTT (+10 mV) suggests that the level of spontaneous disulfide bond formation in V246C channels is incomplete.

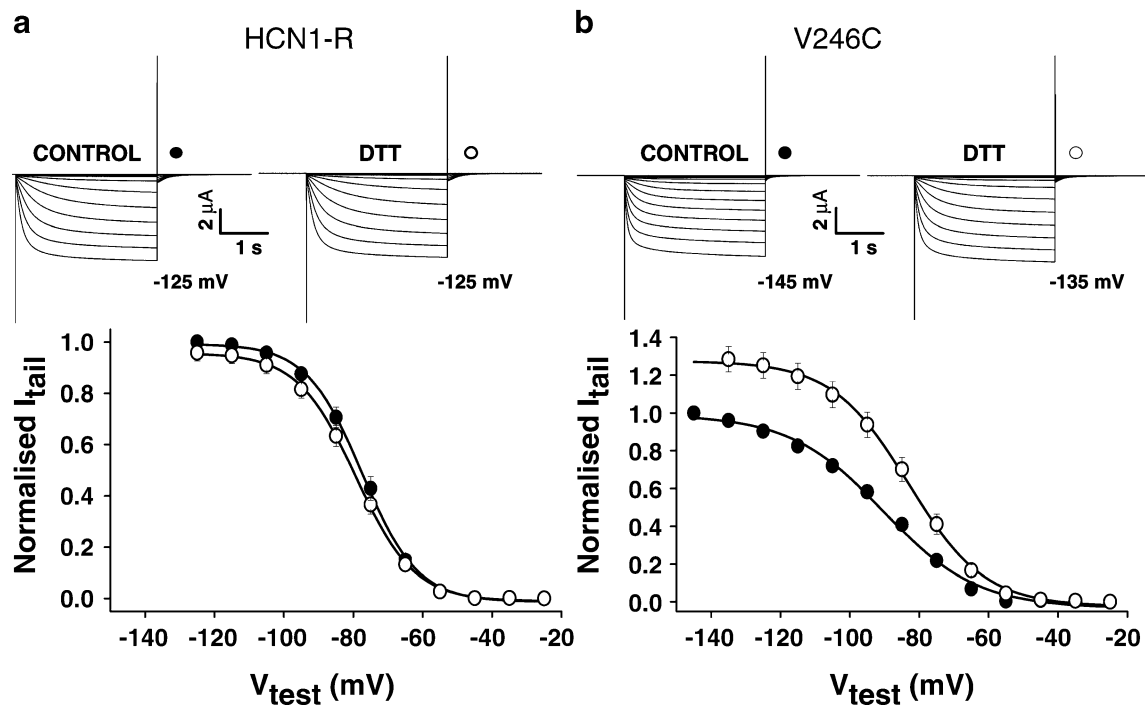


Fig. 1 DTT treatment reveals spontaneous disulfide bridging in V246C but not in HCN1-R channels (C303 alone). Representative TEVC current recordings (*upper panels*) and mean steady-state tail current activation curves (*lower panels*) obtained from cells expressing HCN1-R (**a**) or V246C (**b**) channels. In both cases, cells were maintained in DTT-free Barth's solution. Currents were measured before (*control*) and after (*DTT*) acute exposure to DTT (10 mM) applied by bath perfusion for 3 min in response to the *I*-*V* protocol described in "Materials and methods". In this and subsequent figures, the most negative voltage activation potential is indicated next to the current records. In the lower panels, the *smooth lines* show best fits of

the Boltzmann equation to the mean \pm SEM tail current activation data wherein the $V_{1/2}$, slope (both in mV), and number of observations before (control) and after (post-DTT) were HCN1-R control -77.6 ± 1.5 , 7.9 ± 0.5 ($n=4$, **a**, filled circles); HCN1-R post-DTT -79.3 ± 1.4 , 8.3 ± 0.4 ($n=4$, **a**, open circles); V246C control -90.6 ± 1.5 , 13.4 ± 0.5 ($n=10$, **b**, filled circles); V246C post-DTT -83.7 ± 1.3 , 10.1 ± 0.5 ($n=10$, **b**, open circles). In HCN1-R, neither the $V_{1/2}$ nor slope were significantly affected by DTT ($p=0.074$ and 0.11 , respectively, by paired Student's *t* test) while in V246C, DTT significantly affected both parameters with $p=0.001$ for $V_{1/2}$ and 1.4×10^{-4} for slope (paired Student's *t* test)

V246C channels preferentially coordinate Cd^{2+} in the closed state of the channel

Although the formation of a disulfide bond suggests the reactive sulfhydryls are in close proximity, cross-linking between residues wherein the mean C α to C α distances are up to 15 Å apart have been observed depending on the intrinsic flexibility and mobility of the protein due to thermal fluctuations [10]. To characterize more precisely the proximity of Cys residues in V246C, we examined the effects of extracellular Cd^{2+} on channel function (Fig. 3), as high-affinity coordination of metal ions by two or more Cys sulfhydryl groups occurs only when the distance between Cys α -carbons is <6 Å [11, 42].

HCN1-R currents were unaltered by a >2 -min application of $30 \mu\text{M}$ Cd^{2+} , with no change in the tail current activation curve (mean control $V_{1/2} = -75.9$ mV, $n=5$ versus mean with Cd^{2+} $V_{1/2} = -74.1$, $n=5$; nonsignificant difference $p > 0.05$ with paired Student's *t* test; Fig. 3a). This lack of effect of Cd^{2+} suggests that the C303 residues in each of the four HCN1-R subunits do not come into sufficient

proximity to trap and coordinate Cd^{2+} , in agreement with the failure of these channels to form disulfide bonds. In contrast, V246C channels, were very sensitive to Cd^{2+} , showing a significant ~ 20 mV hyperpolarizing shift in their activation curves in response to a 2-min application of $2 \mu\text{M}$ Cd^{2+} (mean control $V_{1/2} = -78$ mV, $n=4$, versus mean with Cd^{2+} $V_{1/2} = -97.1$ mV, $n=4$; significant difference $p < 0.01$ with paired Student's *t* test), a concentration 15-fold lower than those having no effect on HCN1-R (Fig. 3b). The hyperpolarizing effect of Cd^{2+} on channel activation is similar to the effect seen with disulfide bond formation. Thus, our data are consistent with the view that V246C channels contain pairs of Cys residues in close proximity and that either formation of disulfide bridges or Cd^{2+} coordination between these residues has an inhibitory effect on channel opening.

Does the distance between the Cys residues that coordinate Cd^{2+} change during channel gating? To investigate this question, we compared the rate of Cd^{2+} action when the membrane was held either at a negative voltage for most of a voltage clamp duty cycle so that channels are

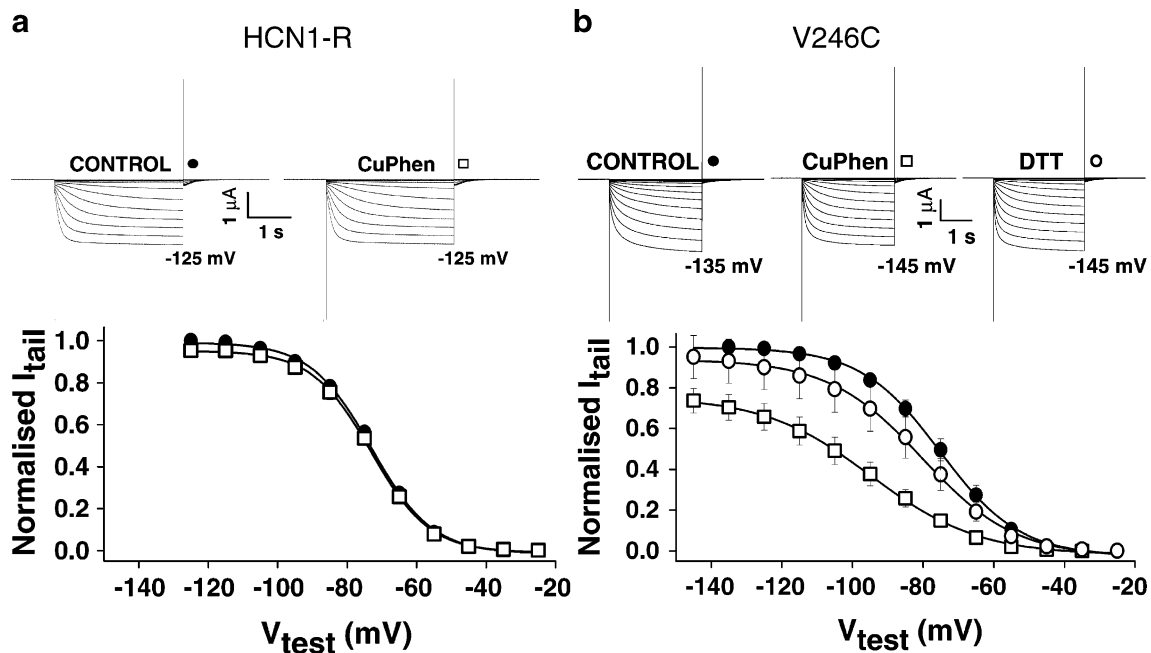


Fig. 2 Cu-phenanthroline (*CuPhen*) treatment induces disulfide bridge formation in V246C but not in HCN1-R (C303 alone) channels. Representative TEVC current recordings (*upper panels*) and mean steady-state tail current activation curves (*lower panels*) obtained from cells expressing HCN1-R (**a**) or V246C (**b**) channels. In both cases, cells were maintained in Barth's solution supplemented with DTT to prevent spontaneous formation of disulfide bonds. Records were obtained before (*control*) and after acute exposure to *CuPhen* (30 μ M for 2 min) in DTT-free recording solution. Following collection of the *CuPhen*-treated *I*–*V* relationship, V246C channels were reexposed to DTT (10 mM for 5–8 min) after which another *I*–*V* relationship was collected (DTT in **b**). Smooth lines in the lower

panels represent fits of the Boltzmann equation to the mean \pm SEM tail current activation data wherein $V_{1/2}$, slope (both in mV) and number of observations were HCN1-R control -73.2 ± 0.6 , 8.8 ± 0.7 ($n=4$, **a**, filled circles); HCN1-R post-*CuPhen* -73.3 ± 0.7 , 8.5 ± 0.6 mV ($n=4$, **a**, open squares); V246C control -75.1 ± 1.6 , 10.7 ± 1.1 ($n=5$, **b**, filled circles); V246C post-*CuPhen* -95.9 ± 2.9 , 14.7 ± 0.7 ($n=5$, **b**, open squares); and V246C post-DTT -82 ± 3.6 , 12.7 ± 0.6 ($n=5$, **b**, open circles). In HCN1-R, neither $V_{1/2}$ ($p=0.66$) nor slope ($p=0.07$) were significantly altered by exposure to *CuPhen* (paired Student's *t* test) while in V246C, both parameters were found to be significantly altered by *CuPhen* treatment ($p=2 \times 10^{-5}$ and 1.4×10^{-4} for $V_{1/2}$ and slope respectively; paired Student's *t* test)

largely open or at a more depolarized potential so that channels are largely closed (see “Materials and methods” for details). With the “open state” paradigm, the mean Cd^{2+} inhibition (coordination) time constant (measured with 10 μ M Cd^{2+}) was 115 s (Fig. 4; $n=6$). With the “closed state” paradigm, the modification time constant shortened to 68 s in the presence of 2 μ M Cd^{2+} (Fig. 4; $n=6$; significantly faster than with the “open state” paradigm, $p=0.02$) and was too fast to quantify at 10 μ M Cd^{2+} . We did not observe any significant difference in unblock time constants upon Cd^{2+} removal at the two voltages (mean Cd^{2+} unblock time constant for the open state was 24.6 s, $n=5$, versus a closed state time constant of 60.6 s, $n=6$; $p>0.05$; Fig. 4).

In principle, an effect of voltage on the time course of Cd^{2+} action could reflect a direct electrostatic effect of membrane voltage on the strength of Cd^{2+} binding to a site within the membrane field. However, an electrostatic effect should lead to an enhanced rate of Cd^{2+} binding from the external solution upon membrane hyperpolarization, the opposite to the hyperpolarization-dependent slowing we observe experimentally. Thus, we conclude that the more

rapid binding to the channels of Cd^{2+} at positive potentials is caused by a conformational change associated with channel closing that brings the pair of cysteine residues that form the Cd^{2+} coordination site in close proximity. This idea is consistent with our finding that Cd^{2+} (and disulfide bond formation) stabilizes the closed state of the channel relative to the open state (Fig. 3).

Intra- versus intersubunit bridging/coordination in V246C channels

There are three potential arrangements of disulfide bond formation involving V246C and C303: (1) an intersubunit disulfide bond forms between V246C residues in adjacent subunits, (2) an intersubunit disulfide bond forms between V246C and C303 in adjacent subunits, and (3) an intrasubunit disulfide bond forms between V246C and C303 in the same subunit. A fourth possibility, intersubunit bonds between C303 residues, is judged to be unlikely due to the lack of effect of the various cysteine reactive reagents in HCN1-R channels. These possibilities could, in principle, be distinguished by coexpressing subunits that contain a single cysteine at position

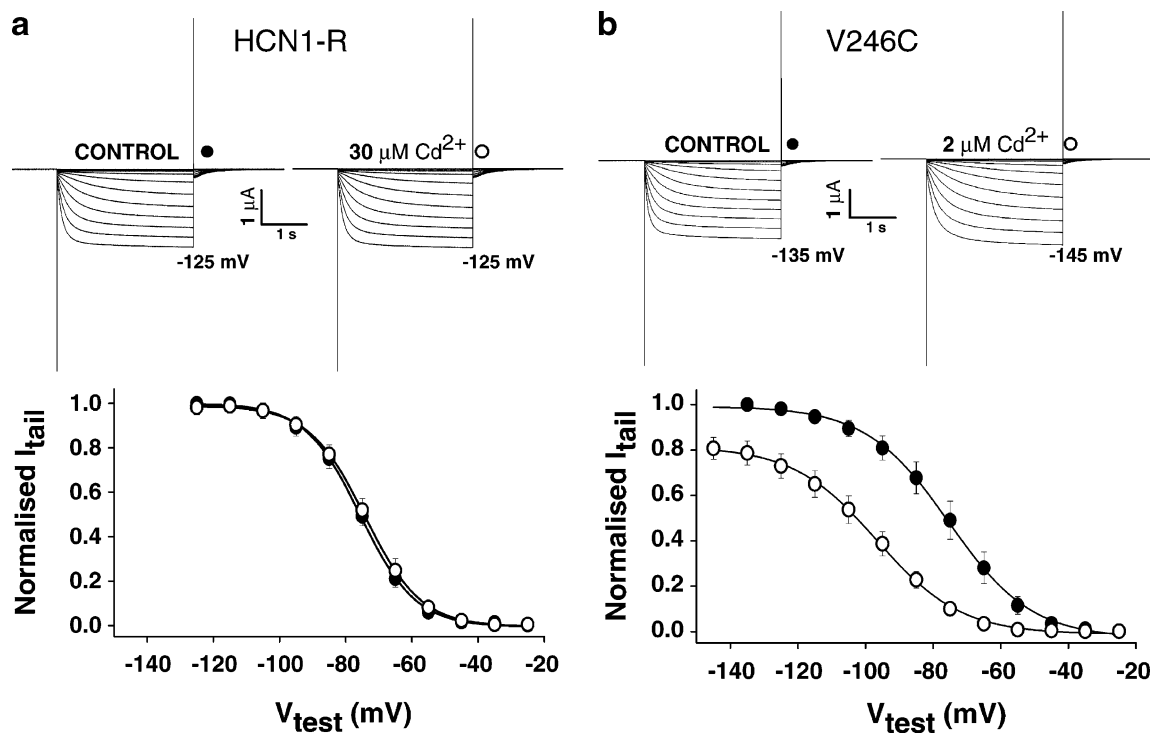


Fig. 3 High-affinity Cd^{2+} binding sites form in V246C but not HCN1-R (C303 alone) channels. Representative TEVC current recordings (*upper panels*) and mean steady-state tail current activation curves (*lower panels*) obtained from cells expressing HCN1-R (**a**) or V246C (**b**) channels. In both cases, cells were maintained in Barth's solution supplemented with DTT to prevent spontaneous formation of disulfide bonds. Records were obtained before (*control*) and after acute exposure to Cd^{2+} for greater than 2 min at the indicated concentrations. Smooth lines in the lower panels represent fits of the Boltzmann equation to the mean \pm SEM tail current activation data

wherein $V_{1/2}$, slope (both in mV) and number of observations were HCN1-R control -75.9 ± 1.8 , 8.4 ± 1.1 ($n=5$, **a**, filled circles); HCN1-R with Cd^{2+} ($30 \mu\text{M}$, applied for >2 min) -74.1 ± 1.6 , 8.4 ± 0.9 ($n=5$, **a**, open circles); V246C control -78 ± 2.9 , 11.8 ± 1 mV ($n=4$, **b**, filled circles); V246C with Cd^{2+} ($2 \mu\text{M}$, applied for >2 min) -97.1 ± 2.4 , 12.2 ± 0.5 ($n=4$, **b**, open circles). In HCN1-R, Cd^{2+} exposure did not significantly alter either gating parameter ($p=0.21$ and 0.89 for $V_{1/2}$ and slope, respectively; paired Student's t test) while in V246C, the $V_{1/2}$ ($p=5 \times 10^{-5}$) but not the slope ($p=0.65$) were significantly altered in the presence of Cd^{2+} (paired Student's t tests)

246 with subunits that contain a single cysteine at residue 303. However, such experiments are precluded as the endogenous cysteine at position 303 cannot be replaced (by any of the 19 other amino acids) without loss of channel function (for further information, see [5]).

To gain insight into the nature of the disulfide bond, we have used an alternative biochemical approach to ask whether CuPhen treatment promotes formation of intersubunit bond formation in the V246C HCN1-R channels (containing C303). This approach is predicated on the following considerations: (1) redox sensitive formation of homotypic or heterotypic *intersubunit* disulfide bridges (between V246C–V246C and C303–V246C, respectively) will result in generation of subunit dimers that will run at a higher molecular weight than monomeric subunits when analyzed on a nonreducing PAGE gel and (2) a redox sensitive formation of a disulfide bond between C303 and V246C within a channel subunit will not markedly alter migration of the channels on a nonreducing PAGE gel.

To assess dimer formation, we initially maintained oocytes in the presence or absence of 0.15 mM DTT.

Forty-eight hours after cRNA injection, we washed out the DTT and exposed a fraction of the DTT-treated oocytes to CuPhen, using incubation conditions comparable to the DTT/CuPhen protocols used in the electrophysiology experiments shown in Fig. 2. Cells were then disrupted under a nitrogen atmosphere using a nitrogen-purged lysis buffer that contained CHAPS and NEM at a pH of 7. These conditions were chosen to minimize the postlysis formation of disulfide bonds. Thus, CHAPS is a small micelle (four–fourteen molecules) dissociating detergent that should separate uncross-linked monomers. The use of pH 7 will retard disulfide bond formation during the initial homogenization while the high concentration of NEM will further suppress postlysis bridge formation by irreversibly alkylating free sulphhydryls.

Figure 5a shows a Western blot analysis of samples extracted from oocytes from three separate donor frogs. The band on the left (ΔC) shows a control experiment using HCN1- $\Delta\text{C}_{\text{term}}$, which contains six endogenous Cys residues. There is a predominant band at $\sim 40 \text{ kD}$ representing the monomeric HCN1- $\Delta\text{C}_{\text{term}}$ species. In addition, there is a significant amount of staining at $\sim 90 \text{ kD}$, representing

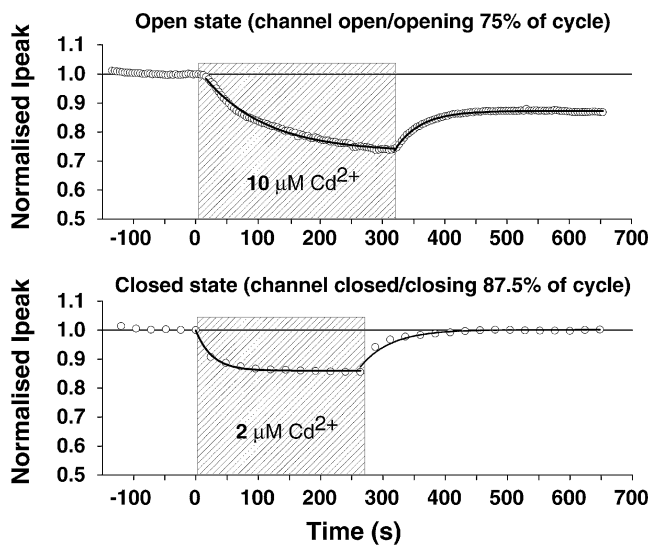


Fig. 4 Cd^{2+} coordination in V246C channels is favored in the channel closed state. Peak amplitude of currents elicited in response to 3 s steps to -125 mV (each normalized to the amplitude of the first step) are plotted as a function of recording time. Cells were maintained in Barth's solution supplemented with DTT to prevent spontaneous formation of disulfide bonds but the recording solution was DTT-free throughout. Hashed boxes indicate the period of Cd^{2+} application. In each case, a single exponential function was fit to the onset and decay of Cd^{2+} action to determine the time constants of block and unblock (see "Materials and methods"). Mean values of time constants when channels were predominantly open were: inhibition time constant = 115 ± 13.4 s ($n=6$, $10 \mu\text{M Cd}^{2+}$) and unblock time constant = 24.6 ± 4.5 s ($n=5$). Time constants when channels were predominantly closed were: inhibition time constant = 68 ± 10.8 s ($n=6$, $2 \mu\text{M Cd}^{2+}$) and unblock time constant = 60.6 ± 17.8 s ($n=5$). The on time constants determined in open and closed channels were significantly different ($p=0.02$) but the off time constants determined were not ($p=0.09$; using Student's t tests). Although, in this example, there is only partial recovery of HCN1 current after washout of $10 \mu\text{M Cd}^{2+}$, on average, there is nearly complete recovery to $92.2 \pm 4.1\%$ of initial current level ($n=5$)

disulfide cross-linked HCN1- $\Delta\text{C}_{\text{term}}$ multimers, indicating that our assay is capable of detecting intersubunit disulfide bond formation. In contrast, V246C HCN1-R subunits are found predominantly as a monomeric species irrespective of the redox treatments prior to cell lysis, suggesting that V246C and C303 participate in an intrasubunit disulfide bond.

The above conclusion is somewhat tempered by our finding that a V246C dimer band can be detected upon overexposure of the gels, although the dimers are present at a much lower level of abundance relative to the monomer band (see the longer exposure shown in the lower panel). The low abundance of the dimer band is consistent with the view that it is a minor protein species, possibly formed under nonphysiological postlysis conditions and that the relevant disulfide bond formed under physiological conditions in intact oocytes is indeed intrasubunit. Alternative-

ly, the minor band of dimers could represent the species relevant to our physiology experiments if only a small fraction of the V246C HCN1-R channels are properly assembled and trafficked to the surface membrane. In this case, the large fraction of monomers could reflect an intracellular pool of immature V246C channels that fail to form disulfide bonds due to the normal reducing environment of the oocyte.

To probe the significance of the V246C dimer band, we examined its sensitivity to treatment with DTT or CuPhen under conditions similar to those used in the electrophysiology experiments. If the minor band of dimers does indeed represent the fraction of channels that are present in the surface membrane, then we expect that the fraction of subunits migrating in the high MW band should be decreased by DTT treatment and increased by CuPhen treatment, similar to the ability of these reagents to regulate channel function in our physiological recordings. We, therefore, measured the density of the dimer band as a percentage of the total channel protein signal (monomer plus dimer). This analysis revealed that pretreatment of oocytes with DTT for 48 h prior to lysis did indeed reduce the fraction of protein in the dimer band by about 50%, compared to the fraction of dimers observed when oocytes were maintained in the absence of DTT. This finding indicates that some intersubunit disulfide bridges in V246C channels do form during the 48-h incubation and so are not simply an artifact of dimer formation during the extraction procedure. However, this result still does not indicate whether the minor fraction of dimers is the relevant species responsible for the physiological effects of the cysteine-reactive reagents.

To address this issue, we next treated intact oocytes with CuPhen and asked whether the catalysis of disulfide bond formation with this reagent is able to increase the fraction of channel protein in the dimer band. If V246C and C303 residues do indeed form an intersubunit bond that is responsible for the dimer band on the gels, then we would expect that CuPhen should increase the fraction of channel protein that appears in this dimer band, similar to the ability of this reagent to alter the functional properties of the channel in our electrophysiological experiments on intact oocytes under similar conditions. However, exposure of oocytes pretreated with DTT to CuPhen had no effect on the density of the dimer band relative to the density observed in the paired DTT-treated samples, despite the ability of this reagent to produce a large 20 mV shift in channel gating under similar conditions. These results are, thus, consistent with the view that CuPhen catalyzes the formation of an *intrasubunit* disulfide bond and, therefore, does not enhance the fraction of protein that appears in the dimer band, which likely represents a physiologically irrelevant channel species. However, we cannot definitively

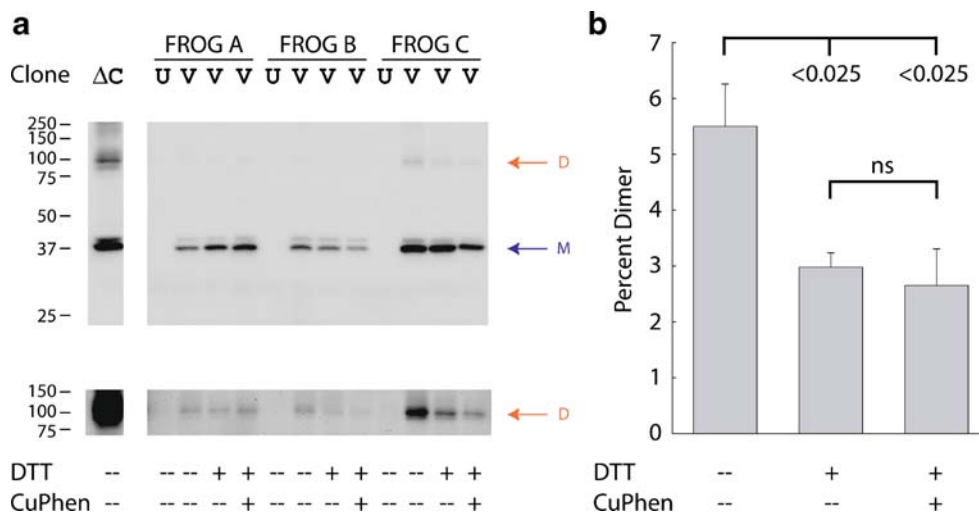


Fig. 5 Reoxidation of V246C with copper phenanthroline does not enhance formation of intersubunit disulfide bonds. **a** Western blot of oocyte lysates obtained from cells injected with HCN1- ΔC_{term} (ΔC), V246C (V), and cells not injected with cRNA (U). The upper image (30 s exposure) shows that V246C is present predominantly as the monomer doublet (blue arrow and M) irrespective of the pretreatment (indicated by the matrix below the lower blot). At this exposure, none of the V246C bands exceeded the bin depth of the camera. The lower image (300-s exposure) shows that dimers (red arrow and D) were present in all V246C lysates. At this exposure, none of the dimer bands exceeded the bin depth of the camera. HCN1- ΔC is included to

show the position of monomers and dimers but exposure times are not optimized to ensure that the signals from this lysate are in the linear range of the imager. **b** Densitometric analysis of blot shown in **a**. Background corrected density for the monomer doublet and dimer were calculated from the 30-s exposures and the dimer density as a function of the total (monomer doublet plus dimer) is shown as mean \pm SEM. Horizontal brackets and text indicate that DTT pretreatment significantly lowered the dimer presence but that this was not reversed by reoxidation with CuPhen as determined by one-way ANOVA analysis (*ns* not significant)

rule out the possibility that CuPhen also catalyzes the formation of intersubunit bonds in some very small fraction of channel protein that is undetectable on our gels

Discussion

Our electrophysiological and biochemical results for HCN1 channels indicate that the extracellular end of S4 comes into close apposition with the adjacent S5 helix in the same subunit when the channels are in the resting closed state. Thus, we observed that disulfide cross-linking and Cd^{2+} coordination between an engineered cysteine at residue 246 in the S4 helix and an endogenous cysteine 303 in the S5 helix stabilize the deactivated closed state of the channel. Moreover, Cd^{2+} coordination between these residues occurs preferentially when the membrane is depolarized, suggesting preferential coordination in the closed state of the channel. Importantly, biochemical studies show that disulfide bond formation is not associated with formation of dimers or higher molecular weight species on a nonreducing gel, suggesting that the disulfide bond is formed between residues within the same subunit. These results provide new information about the state-dependent arrangements of the transmembrane segments in the HCN channel

family and suggest both similarities and differences with the architecture of depolarization-activated Kv channels.

Electrophysiological and biochemical data support an intrasubunit V246C–C303C interaction

Electrophysiological recordings of V246C channels, which contain two Cys residues per subunit (V246C in S4 and C303 in S5), demonstrate robust and complementary effects of reagents that interact with sulfhydryl groups. Treatment with the reducing agent DTT enhanced channel opening by shifting its voltage dependence of activation to more positive potentials, providing evidence for spontaneously formed disulfide bonds that inhibit channel opening. In contrast, application of CuPhen, which catalyzes the formation of disulfide bonds, inhibited channel function by shifting channel activation to more negative potentials. For channels pretreated with DTT to reduce spontaneous disulfide bonds, CuPhen produced a hyperpolarizing shift of ~ 20 mV. Application of Cd^{2+} also inhibited channel function by shifting the voltage dependence of activation by a similar amount. None of these effects were seen with HCN1-R channels that contain only the endogenous C303 residue. Thus, V246C is likely to lie within 6 Å of either C303 or a second V246C residue in a neighboring subunit. Moreover, the metal coordination site involving V246C is

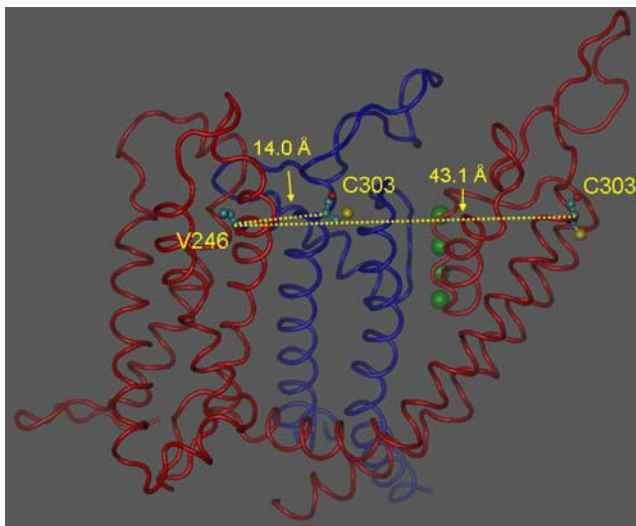


Fig. 6 Model for HCN1 structure based on X-ray crystal structure of Kv1.2. Intra- and intersubunit distances between V246 and C303 in the HCN1 channel were determined using a homology model based on the crystal structure of Kv1.2–Kv2.1 [33]. To simplify the presentation, only one subunit containing S1–S6 (red) and a neighboring subunit containing S5–S6 (blue) are shown. Four K⁺ ions in the selectivity filter are shown as green balls. V246 in the S4 segment together with the C303 residue in S5 of that same subunit and a C303 residue of a neighboring subunit are shown as ball-and-stick figures. The two dashed lines represent the atomic distances between the C- α atoms of V246 and C303 of the same subunit (43.1 Å) and C303 of neighboring subunit (14.0 Å), respectively

preferentially formed when the membrane is depolarized and channels are in the closed state.

The electrophysiology data alone do not allow us to determine whether the Cys–Cys interactions represent an *intersubunit* bond between two V246C residues, an *intersubunit* bond between V246C and C303 in neighboring subunits, or an *intrasubunit* bond between V246C and C303. Western blot analysis of extracted channel protein under nonreducing conditions showed that the predominant species is monomeric (although a small fraction of total protein does exist as dimers, see below). The lack of a prominent dimeric species argues that the majority of disulfide bonds in functional channels must occur in an *intrasubunit* manner between V246C and C303.

As this conclusion is based on a negative result, we need to consider alternative explanations for the lack of dimer formation. Because we find that the distance between V246C and C303 is increased when the channels are in the open state (membrane is hyperpolarized), disulfide bond formation might not occur in the biochemical experiments if the channels were predominantly in the active state. However, we find that disulfide bonds form spontaneously during incubation conditions similar to those used in the biochemical experiments, based on our functional data that DTT treatment enhances channel opening. Moreover, the

majority of V246C channels should be in the closed state at the typical oocyte resting potential (−30 to −50 mV) under our postinjection incubation conditions (Fig. 1).

A second potential complicating factor could occur if only a minor fraction of the total V246C protein on the Western blots represents functional channels expressed in the surface membrane. Any pool of intracellular channel protein might be unable to form disulfide bonds due to the reducing environment of the oocyte. As a result, only a small fraction of the total protein would be able to form dimers, even if V246C participates in an intersubunit disulfide bond. Although it is difficult to address this problem definitively, we *can* readily detect significant multimer formation in HCN1- ΔC_{term} , which contains six endogenous Cys residues and is the parent construct for HCN1-R. Importantly, we also found that the dimer signal in the V246C channel Western blots is unaffected by pretreatment of oocytes with CuPhen (Fig. 5), despite the ability of this reagent to catalyze disulfide bond formation in V246C channels expressed in the surface membrane. This suggests that the small amount of dimer formation in these channels represents a rare event that is not representative of the conformation of the fully assembled channel in the surface membrane, e.g., possibly an artifactual intersubunit proximity of Cys–Cys residues arising during oocyte homogenization and protein extraction. However, it is important to point out that our results do not rule out the formation of physiologically relevant intersubunit bonds that are below the limits of detection of our biochemical experiments.

Accounting for the closer proximity of S4 and S5 helices during membrane depolarization

Both the state dependence of Cd²⁺ binding and the effect of Cd²⁺ and disulfide bonds to inhibit channel opening suggest that V246C and C303 within the same subunit are in close proximity when the membrane is depolarized and the channels are closed. Previous data suggests that there are minimal vertical transmembrane motions of the S4 helix during voltage sensing and gating of mammalian HCN channels and that V246C remains readily accessible to the external aqueous environment in both closed and open states of the channel [5, 50]. These results together suggest that protein motions during membrane depolarization that account for the state-dependent interaction of V246 and C303 may involve a lateral translation or rotation in the plane of the membrane, bringing the top of S4 in closer proximity to S5 of the same subunit. Such a lateral motion could be explained by tilting of S4 relative to S5, consistent with the previous S4 accessibility studies on mammalian HCN channels [5]. Alternatively, a transmembrane motion of S5 might move C303 in closer proximity to S4 during membrane depolarization. Presumably, the curtailing of

such motions by disulfide bridging or Cd^{2+} coordination between the S4 and S5 helices give rise to the observed inhibition of channel opening and shift of gating to more negative potentials.

Comparison of S4–S5 topology between HCN channels and depolarization-activated Kv channels

Hyperpolarization-activated HCN channels are members of the Kv channel superfamily and, like other family members, contain six transmembrane segments, a positively charged S4 segment that is part of the S1–S4 voltage-sensing domain and a pore-forming S5–S6 region. Previously, we found that the voltage-sensing mechanism in mammalian HCN channels [5] shares some key elements with the transporter model for voltage sensing [7, 14, 48], one of three putative gating models hypothesized for depolarization-activated Kv channels (see “Introduction” for a summary). Thus, HCN channels appear to display a highly focused electric field due to aqueous crevices and membrane deformation around S4 and exhibit small transmembrane motions (<3 Å) of S4.

The state-dependent changes in the S4–S5 arrangement seen here for HCN1 channels show intriguing similarities and differences with *Shaker* Kv channels [8, 18, 25, 36]. Thus, certain pairs of *Shaker* residues near the extracellular ends of S4 and S5 form *intersubunit* disulfide bonds and Cd^{2+} coordination sites [8, 25, 36]. In contrast, Elliott et al. [18] found that a different pair of *Shaker* residues near the external ends of S4 and S5 form an *intrasubunit* Cd^{2+} coordination site preferentially when the channels are activated by depolarization. Of particular interest, this same pair of *Shaker* residues forms an *intersubunit* interaction when the channels are in the resting state (membrane hyperpolarized). From these results, Elliott et al. [18] concluded that the top of S4 lies near the top of S5 of an adjacent subunit in the resting state; during channel activation, there is a conformational change that causes the top of S4 to lie near the top of S5 in the same subunit. Furthermore, studies in the hyperpolarization-activated KAT1 channel suggest the possibility of three residue pairings along the lengths of S4 and S5, including possibly both intra- and intersubunit interactions, which arise during channel gating [21, 24].

The above results demonstrate that in HCN1, KAT1 and *Shaker* channels S4 and S5 within the same subunit may move into close proximity during voltage sensing motions when the membrane is depolarized, even though *Shaker* channels are in the open state at this potential whereas HCN1 and KAT1 channels are in the closed state. Thus, the orientation of the S4 and S5 segments is likely to reflect the state of the voltage sensor (which is a function of membrane potential) rather than the state of the channel

gate. That HCN1 channels may not form the intersubunit Cd^{2+} coordination site seen in Kv channels at hyperpolarized potentials is consistent with the notion that the S4 segments in HCN1 channels show a more restricted motion during voltage sensing compared to the S4 segments of Kv channels [5, 50].

The finding that S4 and S5 in the same subunit are in close proximity when the membrane is depolarized is difficult to reconcile with the X-ray crystal structure of the homologous mammalian Kv1.2 channel [31], where the S1–S4 voltage-sensing subdomain lies close to the S5 segment of a neighboring subunit but far from its own S5 segment. Although the structure is somewhat more compatible with the finding of *intersubunit* interactions between residues at the top of S4 and S5 in *Shaker* channels [8, 18, 25], even here, a discrepancy exists as the *Shaker* channel S4–S5 intersubunit interactions occur preferentially in the resting state [18], whereas the X-ray structure is of the open channel. Moreover, the intersubunit distance between the top of S4 and S5 in the crystal structure is too great to explain high-affinity metal coordination [27].

To gain more insight as to whether the distance between V246C and C303 in HCN1 is compatible with the Kv1.2 structure, we modeled HCN1 based on the Kv1.2 structure using a multiple sequence alignment (Fig. 6). As there is some ambiguity in the alignments, we explored structures based on four distinct possible alignments. The intrasubunit distances between V246C and C303 ranged from 33–43 Å in the four structures, all too large to support formation of disulfide bonds or coordinate Cd^{2+} binding. The intersubunit distances, ranging from 14–23 Å, are less than the intrasubunit distances but are still at the upper limit for disulfide bond formation and too large to form a high-affinity Cd^{2+} binding site. Thus, the structure of HCN1 may differ substantially from that of Kv1.2. Alternatively, the Kv1.2 structure may be partially distorted [27]. Finally, the V246C–C303 intrasubunit disulfide bonds or Cd^{2+} coordination may occur during rare sojourns of the HCN1 channel into a distorted state that becomes trapped by covalent bond formation or Cd^{2+} binding. However, any such distortion cannot be too great as the 20 mV shift in voltage gating represents a relatively modest functional change.

Given the apparent similarities in channel architecture identified here that give rise to intrasubunit interactions between S4 and S5 in depolarization activated Kv channels and the hyperpolarization-activated HCN1 (and potentially also in KAT1) channels, our results argue that the opposite polarity of voltage sensitivity arises elsewhere in the HCN channel structure. This could occur at the intracellular side of the membrane where the S4–S5 linker is thought to couple voltage-sensor movement to channel gating [15, 16, 40]. Alternatively, HCN1 voltage-gating polarity could be

determined by conformational changes in the channel regions surrounding S4 as described previously [5, 50].

Acknowledgements We thank Keri Fogle and Renee Saenger for technical assistance and Margaret Wood and the Department of Anesthesiology for continuing support. D.C.B. was supported by the Wellcome Trust (UK) and an American Heart Association grant (0325454T). S.A.S. was supported by the Howard Hughes Medical Institute and grant R01NS36658 from the National Institutes of Health. G.R.T. was supported by The Whitehall Foundation (2003-05-02-REN).

Open Access This article is distributed under the terms of the Creative Commons Attribution Noncommercial License which permits any noncommercial use, distribution, and reproduction in any medium, provided the original author(s) and source are credited.

References

- Ahern CA, Horn R (2004) Specificity of charge-carrying residues in the voltage sensor of potassium channels. *J Gen Physiol* 123:205–216
- Ahern CA, Horn R (2005) Focused electric field across the voltage sensor of potassium channels. *Neuron* 48:25–29
- Au KW, Siu CW, Lau CP, Tse HF, Li RA (2008) Structural and functional determinants in the S5-P region of HCN-encoded pacemaker channels revealed by cysteine-scanning substitutions. *Am J Physiol Cell Physiol* 294:C136–144
- Baker OS, Larsson HP, Mannuzzu LM, Isacoff EY (1998) Three transmembrane conformations and sequence-dependent displacement of the S4 domain in shaker K⁺ channel gating. *Neuron* 20:1283–1294
- Bell DC, Yao H, Saenger RC, Riley JH, Siegelbaum SA (2004) Changes in local S4 environment provide a voltage-sensing mechanism for mammalian hyperpolarization-activated HCN channels. *J Gen Physiol* 123:5–19
- Bezanilla F (2000) The voltage sensor in voltage-dependent ion channels. *Physiol Rev* 80:555–592
- Bezanilla F (2005) The voltage-sensor structure in a voltage-gated channel. *Trends Biochem Sci* 30:166–168
- Broomand A, Mannikko R, Larsson HP, Elinder F (2003) Molecular movement of the voltage sensor in a K channel. *J Gen Physiol* 122:741–748
- Campos FV, Chanda B, Roux B, Bezanilla F (2007) Two atomic constraints unambiguously position the S4 segment relative to S1 and S2 segments in the closed state of Shaker K channel. *Proc Natl Acad Sci U S A* 104:7904–7909
- Careaga CL, Falke JJ (1992) Thermal motions of surface alpha-helices in the D-galactose chemosensory receptor. Detection by disulfide trapping. *J Mol Biol* 226:1219–1235
- Castagnetto JM, Hennessy SW, Roberts VA, Getzoff ED, Tainer JA, Pique ME (2002) MDB: the Metalloprotein Database and Browser at The Scripps Research Institute. *Nucleic Acids Res* 30:379–382
- Catterall WA (1986) Molecular properties of voltage-sensitive sodium channels. *Annu Rev Biochem* 55:953–985
- Cha A, Snyder GE, Selvin PR, Bezanilla F (1999) Atomic scale movement of the voltage-sensing region in a potassium channel measured via spectroscopy. *Nature* 402:809–813
- Chanda B, Asamoah OK, Blunck R, Roux B, Bezanilla F (2005) Gating charge displacement in voltage-gated ion channels involves limited transmembrane movement. *Nature* 436:852–856
- Chen J, Mitcheson JS, Tristani-Firouzi M, Lin M, Sanguinetti MC (2001) The S4–S5 linker couples voltage sensing and activation of pacemaker channels. *Proc Natl Acad Sci U S A* 98:11277–11282
- Decher N, Chen J, Sanguinetti MC (2004) Voltage-dependent gating of hyperpolarization-activated, cyclic nucleotide-gated pacemaker channels: molecular coupling between the S4–S5 and C-linkers. *J Biol Chem* 279:13859–13865
- Elinder F, Nilsson J, Arhem P (2007) On the opening of voltage-gated ion channels. *Physiol Behav* 92:1–7
- Elliott DJ, Neale EJ, Aziz Q, Dunham JP, Munsey TS, Hunter M, Sivaprasadarao A (2004) Molecular mechanism of voltage sensor movements in a potassium channel. *EMBO J* 23:4717–4726
- Giorgetti A, Carloni P, Mistrik P, Torre V (2005) A homology model of the pore region of HCN channels. *Biophys J* 89:932–944
- Glauner KS, Mannuzzu LM, Gandhi CS, Isacoff EY (1999) Spectroscopic mapping of voltage sensor movement in the Shaker potassium channel. *Nature* 402:813–817
- Grabe M, Lai HC, Jain M, Jan YN, Jan LY (2007) Structure prediction for the down state of a potassium channel voltage sensor. *Nature* 445:550–553
- Guy HR, Seetharamulu P (1986) Molecular model of the action potential sodium channel. *Proc Natl Acad Sci U S A* 83:508–512
- Jiang Y, Ruta V, Chen J, Lee A, MacKinnon R (2003) The principle of gating charge movement in a voltage-dependent K⁺ channel. *Nature* 423:42–48
- Lai HC, Grabe M, Jan YN, Jan LY (2005) The S4 voltage sensor packs against the pore domain in the KAT1 voltage-gated potassium channel. *Neuron* 47:395–406
- Laine M, Lin MC, Bannister JP, Silverman WR, Mock AF, Roux B, Papazian DM (2003) Atomic proximity between S4 segment and pore domain in Shaker potassium channels. *Neuron* 39:467–481
- Larsson HP, Baker OS, Dhillon DS, Isacoff EY (1996) Transmembrane movement of the shaker K⁺ channel S4. *Neuron* 16:387–397
- Lewis A, Jogini V, Blachowicz L, Laine M, Roux B (2008) Atomic constraints between the voltage sensor and the pore domain in a voltage-gated K⁺ channel of known structure. *J Gen Physiol* 131:549–561
- Liman ER, Hess P, Weaver F, Koren G (1991) Voltage-sensing residues in the S4 region of a mammalian K⁺ channel. *Nature* 353:752–756
- Liman ER, Tytgat J, Hess P (1992) Subunit stoichiometry of a mammalian K⁺ channel determined by construction of multimeric cDNAs. *Neuron* 9:861–871
- Logothetis DE, Movahedi S, Satler C, Lindpaintner K, Nadal-Ginard B (1992) Incremental reductions of positive charge within the S4 region of a voltage-gated K⁺ channel result in corresponding decreases in gating charge. *Neuron* 8:531–540
- Long SB, Campbell EB, MacKinnon R (2005) Crystal structure of a mammalian voltage-dependent Shaker family K⁺ channel. *Science* 309:897–903
- Long SB, Campbell EB, MacKinnon R (2005) Voltage sensor of Kv1.2: structural basis of electromechanical coupling. *Science* 309:903–908
- Long SB, Tao X, Campbell EB, MacKinnon R (2007) Atomic structure of a voltage-dependent K⁺ channel in a lipid membrane-like environment. *Nature* 450:376–382
- Ludwig A, Zong X, Jeglitsch M, Hofmann F, Biel M (1998) A family of hyperpolarization-activated mammalian cation channels. *Nature* 393:587–591
- Männikkö R, Elinder F, Larsson HP (2002) Voltage-sensing mechanism is conserved among ion channels gated by opposite voltages. *Nature* 419:837–841
- Neale EJ, Elliott DJ, Hunter M, Sivaprasadarao A (2003) Evidence for intersubunit interactions between S4 and S5

- transmembrane segments of the Shaker potassium channel. *J Biol Chem* 278:29079–29085
37. Papazian DM, Timpe LC, Jan YN, Jan LY (1991) Alteration of voltage-dependence of Shaker potassium channel by mutations in the S4 sequence. *Nature* 349:305–310
 38. Pathak MM, Yarov-Yarovoy V, Agarwal G, Roux B, Barth P, Kohout S, Tombola F, Isacoff EY (2007) Closing in on the resting state of the Shaker K(+) channel. *Neuron* 56:124–140
 39. Posson DJ, Ge P, Miller C, Bezanilla F, Selvin PR (2005) Small vertical movement of a K⁺ channel voltage sensor measured with luminescence energy transfer. *Nature* 436:848–851
 40. Prole DL, Yellen G (2006) Reversal of HCN channel voltage dependence via bridging of the S4–S5 linker and post-S6. *J Gen Physiol* 128:273–282
 41. Robinson RB, Siegelbaum SA (2003) Hyperpolarization-activated cation currents: from molecules to physiological function. *Annu Rev Physiol* 65:453–480
 42. Rulisek L, Vondrasek J (1998) Coordination geometries of selected transition metal ions (Co²⁺, Ni²⁺, Cu²⁺, Zn²⁺, Cd²⁺, and Hg²⁺) in metalloproteins. *J Inorg Biochem* 71:115–127
 43. Ruta V, Chen J, MacKinnon R (2005) Calibrated measurement of gating-charge arginine displacement in the KvAP voltage-dependent K⁺ channel. *Cell* 123:463–475
 44. Sambrook J, Fritsch EF, Maniatis T (1989) Molecular cloning. A laboratory manual. Cold Spring Harbor Laboratory, Cold Spring Harbor, NY
 45. Santoro B, Liu DT, Yao H, Bartsch D, Kandel ER, Siegelbaum SA, Tibbs GR (1998) Identification of a gene encoding a hyperpolarization-activated pacemaker channel of brain. *Cell* 93:717–729
 46. Santoro B, Tibbs GR (1999) The HCN gene family: molecular basis of the hyperpolarization-activated pacemaker channels. *Ann N Y Acad Sci* 868:741–764
 47. Sesti F, Rajan S, Gonzalez-Colaso R, Nikolaeva N, Goldstein SA (2003) Hyperpolarization moves S4 sensors inward to open MVP, a methanococcal voltage-gated potassium channel. *Nat Neurosci* 6:353–361
 48. Starace DM, Bezanilla F (2004) A proton pore in a potassium channel voltage sensor reveals a focused electric field. *Nature* 427:548–553
 49. Tombola F, Pathak MM, Isacoff EY (2006) How does voltage open an ion channel? *Annu Rev Cell Dev Biol* 22:23–52
 50. Vemana S, Pandey S, Larsson HP (2004) S4 movement in a mammalian HCN channel. *J Gen Physiol* 123:21–32
 51. Yang N, George AL Jr, Horn R (1996) Molecular basis of charge movement in voltage-gated sodium channels. *Neuron* 16:113–122
 52. Yarov-Yarovoy V, Baker D, Catterall WA (2006) Voltage sensor conformations in the open and closed states in ROSETTA structural models of K(+) channels. *Proc Natl Acad Sci U S A* 103:7292–7297
 53. Yusaf SP, Wray D, Sivaprasadarao A (1996) Measurement of the movement of the S4 segment during the activation of a voltage-gated potassium channel. *Pflugers Arch* 433:91–97